Source term considerations in connection with chemical accidents and vapour cloud modelling

Hans K. Fauske and Michael Epstein
Fauske & Associates, Inc., 16W070 West 83rd Street, Burr Ridge, IL 60521, USA

Source term considerations involving flashing two-phase high momentum releases are presented in terms of simple models. These include methods for assessing discharge rates for subcooled, saturated and two-phase stagnation conditions, expanded jet behaviour including aspects of entrainment, vapourization and cooling as well as the extent of the two-phase jet regime. The models are compared with applicable experimental data including the large scale ammonia and hydrofluoric acid jet releases performed on the Frenchman Flat area of the Department of Energy's Nevada Test Site.

(Keywords: two phase flow; momentum turbulence; modelling)

Rare, but major and dangerous chemical releases are usually related to overpressure scenarios and venting in connection with runaway chemical reactions and/or fire exposure and accidental breaches in vessel pipe works containing toxic and flammable liquids. Examples of such controlled releases include the SEVESO incident in Italy in 1976, in which dioxins were discharged into the air through the Emergency Relief System (ERS); the Farmland Industries release to the atmosphere in 1981 of 40 tons of ammonia through the ERS on a storage tank; and the Bhopal incident in 1984, which led to a large release of methyl isocyanate due to a largely ineffective scrubbing system. The frequency of uncontrolled releases, i.e. explosions as a result of inadequate vent size designs can be further reduced by adopting the methodology recently completed by the AIChE DIERS programme[1].

The growing realization that most emergency releases involve high momentum two-phase discharges even in cases of controlled releases, has led to increased interest in modelling such jet releases. In this paper, simple models for estimating source term related phenomena including the discharge rate, the extent and properties associated with the jet depressurization as well as the intensive exchange of mass with the atmosphere following depressurization are presented. The models are compared with applicable data including the results of large scale pressurized ammonia and hydrofluoric acid release tests performed on the Frenchman Flat area of the Department of Energy's Nevada Test Site. For the latter tests, quantities of interest include the source rate, the length of the two-phase jet prior to complete ammonia and hydrofluoric acid vapourization as well as the strong cooling associated with the evaporation process. The effects of water vapour condensation and subsequent re-vapourization have not yet been studied. The observed persistence of visible plumes may be due to condensation of the atmospheric water content.

Received 4 January 1988

0950-4230/88/020075-09$3.00

Modelling of source flow rates

In the absence of significant frictional losses the flashing flows through ducts are generally choked, and in many applications the critical pressure can be approximated by the vapour pressure corresponding to the stagnation temperature[2]. As illustrated below, this assumption allows simple models to be formulated to estimate the source flow rate. These models agree rather well with experimental observations.

Subcooled stagnation conditions

For vessel conditions where the stagnation pressure is substantially larger than the vapour pressure corresponding to the stagnation temperature, the above assumption suggests that an all-liquid Bernoulli type flow can be assumed to calculate the flow rate:

$$G = c_d\sqrt{2[P_0 - P_v(T_0)]\rho_f} \quad (1)$$

where c_d is the discharge coefficient; P_0 is the stagnation pressure; $P_v(T_0)$ is vapour pressure at stagnation temperature T_0; and ρ_f is the liquid density.

Equation (1) compares well with data such as the results of large scale pressurized amonia[3] and hydrofluoric acid[4] release tests performed on the Frenchman Flat area of the Department of Energy's Nevada Test Site. For example, liquid ammonia at $T_0 = 297$ K (24°C)

Table 1 Examples of measured and calculated flow rates for ammonia and hydrofluoric acid spills

Fluid	P_0 (Pa)	$P_v(T_0)$ (Pa)	Flow rate ($m^3 min^{-1}$) Measured	Calculated
NH_3	1.4×10^6	0.97×10^6	8.5	9.5
HF	8.67×10^5	2.07×10^5	1.78	1.83
HF	9.08×10^5	2.07×10^5	0.65	0.63

and pressurized to $P_0 = 1.4 \times 10^6$ Pa (203 psia) was allowed to escape from a tanker truck through a 0.0945 m diameter orifice plate. The vapour pressure of ammonia at $T_0 = 24°C$ is $P_v(T_0) = 0.968 \times 10^6$ Pa. Thus the ammonia is discharged from a subcooled stagnation state, and the calculated flow rate from Equation (1) becomes:

$$G = 0.6\sqrt{2 \times [1.4 \times 10^6 - 0.968 \times 10^6] \times 603}$$
$$\approx 1.36 \times 10^4 \text{ kg m}^{-2}\text{s}$$

The volume discharge rate through the orifice plate is then:

$$\frac{GA}{\rho_f} = \frac{(1.36 \times 10^4)(0.007)}{603}$$
$$\approx 0.158 \text{ m}^3 \text{ s}^{-1} \approx 9.5 \text{ m}^3 \text{ min}^{-1}$$

This prediction is close to the measured volumetric discharge rate of 8.5 $m^3 min^{-1}$. Comparisons for both the ammonia and hydrofluoric acid spill tests are summarized in *Table 1*.

As the subcooling approaches zero, i.e. as P_0 approaches $P_v(T_0)$, Equation (1) needs to be modified as discussed further below.

Saturated stagnation conditions

For saturated liquid conditions, $P_0 = P_v(T_0)$, the choked flow rate can be expressed as:

$$G = \left(\frac{-1}{(dv/dP)}\right)^{1/2} \tag{2}$$

where v is the two-phase specific volume given by:

$$v = v_{fg}x + v_f \tag{3}$$

where: v_{fg} is the change in specific volume going from liquid to vapour; v_f is the liquid specific volume; and x is the vapour quality. Note that Equation (3) implies homogeneous flow conditions, i.e. equal vapour and liquid velocities.

For low quality flashing liquid conditions, the change in specific volume with respect to pressure can be approximated as:

$$\frac{dv}{dP} \approx v_{fg}\frac{dx}{dP} \approx -v_{fg}\frac{c}{h_{fg}}\frac{dT}{dP} \approx \frac{v_{fg}^2}{h_{fg}^2}Tc \tag{4}$$

where c is the liquid specific heat and h_{fg} is the latent heat of vapourization. Equation (4) is a reasonable approximation as long as the following inequality is satisfied:

$$x < \frac{Pv_{fg}}{h_{fg}^2}Tc \tag{5}$$

Substituting Equation (4) into Equation (2) one obtains the following simple expressions for the choked mass flow rate:

$$G \approx \frac{h_{fg}}{v_{fg}}\left(\frac{1}{Tc}\right)^{1/2} \approx \frac{dP}{dT}\left(\frac{T}{c}\right)^{1/2} \tag{6}$$

As noted in the beginning of this discussion, in the absence of frictional losses, the critical pressure ratio for equilibrium flashing can be assumed equal to 1, i.e. the flow rate given by Equation (6) can be simply evaluated based upon stagnation properties.

Examples of such equilibrium calculations are provided in *Table 2* for several hazardous systems of interest. For propylene, the flow rate is calculated to be

$$G \approx \frac{3.34 \times 10^5}{0.042}\left(\frac{1}{2.18 \times 10^3 \times 298}\right)^{1/2}$$
$$\approx 9870 \text{ kg m}^{-2}\text{s}$$

As long as inequality (5) is satisfied, the flashing flow rate remains essentially invariant with the inlet vapour quality. For the propylene system, vapour qualities:

$$x < \frac{1.15 \times 10^6 \times 0.042}{(3.34 \times 10^5)} 2.18 \times 10^3 \times 298$$
$$< \approx 0.28$$

will satisfy this condition. This corresponds to an inlet void fraction of:

$$\alpha = \frac{xv_g}{(1-x)v_f + xv_g} \tag{7}$$
$$\approx \frac{0.28 \times 0.044}{(0.72 \times 0.002) + (0.28 \times 0.044)} \approx 0.92$$

As can be seen from *Table 2*, for inlet void fractions of $< \approx 0.9$, the use of Equation (6) will provide a good estimate of the flashing flow rate without the need to specify the liquid-to-vapour phase ratio involved in the discharge. This is most fortunate, since for many

Table 2 Examples of maximum equilibrium flashing flow rates (Equation (6)) for hazardous material. Stagnation pressure equals vapour pressure at 25°C (298 K)

Toxic gas	$P = P_0 = P_v$ (Pa) @ (25°C)	h_{fg} ($J kg^{-1}$)	v_{fg} ($m^3 kg^{-1}$)	c ($J kg^{-1} K$)	Equation (6); G ($kg m^{-2} s$)	Inequality (5) x	Equation (7) α
Propylene	1.15×10^6	3.34×10^5	0.042	2.18×10^3	9870	0.28	0.92
Propane	0.95×10^6	3.33×10^5	0.048	2.23×10^3	8500	0.27	0.90
Ammonia	1×10^6	1.17×10^6	0.127	4.49×10^3	7960	0.13	0.92
Methyl chloride	0.56×10^6	3.75×10^5	0.077	1.5×10^3	7280	0.14	0.92
Sulphur dioxide	0.39×10^6	3.56×10^5	0.09	1.36×10^3	6210	0.11	0.94

chemical systems it is difficult to predict this parameter *a priori* without prior knowledge of the system behaviour under actual accidental conditions. Furthermore, many chemical systems exhibit a frothy or foamy nature under accidental conditions, implying that Equation (6) can be used to calculate the source flow rate as well as the duration of the release.

In the transition region from subcooled to saturated stagnation conditions, the following expression for the choked flow rates suggests itself:

$$G \approx c_d \sqrt{2[P_0 - P_v(T_0)]\rho_f + \frac{h_{fg}^2}{v_{fg}^2}\frac{1}{Tc}} \tag{8}$$

If the subcooling is large, Equation (8) reduces to Equation (1) and if the subcooling is zero Equation (8) simply converts back to Equation (6). Good agreement is obtained between predictions based upon Equation (6), and experimental data such as the large scale water blowdown data carried out in the Marviken facility[2].

Frictional losses. The relationship noted experimentally between the flashing flow rate and the length-to-diameter (L/D) ratio can be calculated on the basis of the well known homogeneous equilibrium model accounting for frictional dissipation[5]. Such calculations can be simplified by introducing a flow reduction factor F in Equation (6) as follows:

$$G \approx F\frac{h_{fg}}{v_{fg}}\left(\frac{1}{Tc}\right)^{1/2} \approx F\frac{dP}{dT}\left(\frac{T}{c}\right)^{1/2} \tag{9}$$

where $F \approx 1$ for $L/D = 0$; $F \approx 0.85$ for $L/D = 50$; $F \approx 0.75$ for $L/D = 100$; $F \approx 0.65$ for $L/D = 200$; and $F \approx 0.55$ for $L/D = 400$; and as before the properties in Equation (9) can be evaluated based upon stagnation conditions.

For many chemical systems of interest, such as controlled releases of runaway chemical reactions, relatively little difference is noted between the flashing flow rates obtained in experiments with top- and bottom-venting[6]. This observation can be related both to the foamy-nature of many chemical systems as well as the invariant nature of the flashing flow rate with large variation in the vessel void fraction as indicated above. A reasonable source flow rate envelope for such systems can be provided by Equation (9) as illustrated in *Figure 1*.

The flow rate for the flashing ethylbenzene-styrene mixture is evaluated as:

$$G \approx (0.5)(8246)\left(\frac{490}{2520}\right)^{1/2}$$

$$\approx 1820\ \mathrm{kg\,m^{-2}\,s}$$

and the duration of the release is given by:

$$\Delta t = \frac{m_0}{GA} \approx \frac{21}{(1820)(1.56\times10^{-4})} \approx 74\ \mathrm{s}$$

where m_0 is the initial mass of reactants and A is the experimental vent area. It is of interest to note that the flashing flow rate given by Equation (9) is also the key

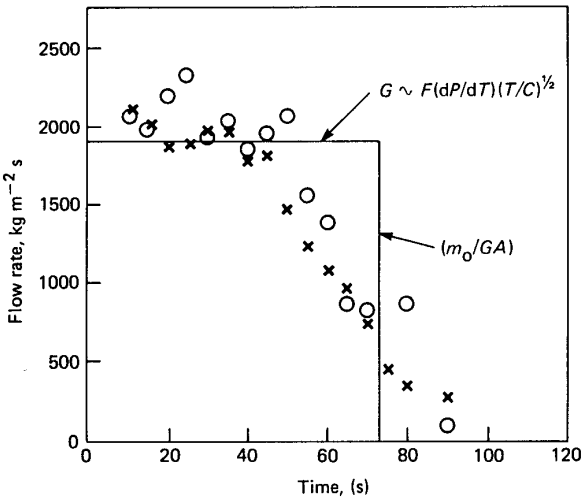

Figure 1 Illustration of recommended source term and comparison with experiments. Little difference is noted between top- and bottom-vented conditions, which is typical for many systems. Data represent controlled venting of a runaway ethylbenzene-styrene reaction ($m_0 = 21$ kg; $P_{set} = 0.515$ MPa and $T_{set} = 490$ K; $D = 14.1$ mm and $L/D \approx 430$) (Ref. 6): ×, top venting; ○, bottom venting

to determining the necessary vent area, A, in order to assure a controlled release[7].

$$A = \frac{1}{2}\frac{m_0(dT/dt)_s(\alpha_D - \alpha_0)}{F(T/c)^{1/2}\,\Delta P(1-\alpha_0)} \tag{10}$$

where $(dT/dt)_s$ is the self-heat rate corresponding to the relief set pressure; α_D is the average vessel void fraction at complete vapour disengagement; α_0 is the void fraction corresponding to the initial free board volume; and ΔP is overpressure, i.e. the equilibrium vapour pressure corresponding to the turnaround temperature minus the relief set pressure.

For the top vented conditions in *Figure 1*, Equation (10) results in the following vent area requirement:

$$A \approx \frac{1}{2}\frac{(21)(0.38)(0.93-0.1)}{(0.5)(490/2500)^{1/2}(1.03\times10^5)(1-0.1)}$$

$$\approx 1.6\times10^{-4} \approx 14.3\ \mathrm{mm}$$

which compares with the experimental vent diameter of 14.1 mm. It follows that the magnitude of the controlled release rate (GA) as well as the duration (m_0/GA) can be predicted quite well from Equations (9) and (10), as long as $(dT/dt)_s$ and (dP/dT) can be specified. If not known, these quantities can be measured in the DIERS bench scale apparatus[1].

Non-equilibrium conditions. Based upon experimental observations, equilibrium flow for saturated inlet conditions are approached for flow lengths >0.1 m (Ref. 2). For flow lengths <0.1 m, the flashing flow increases strongly with decreasing length, approaching all liquid flow as the length approaches zero. This non-equilibrium effect can be estimated by introducing

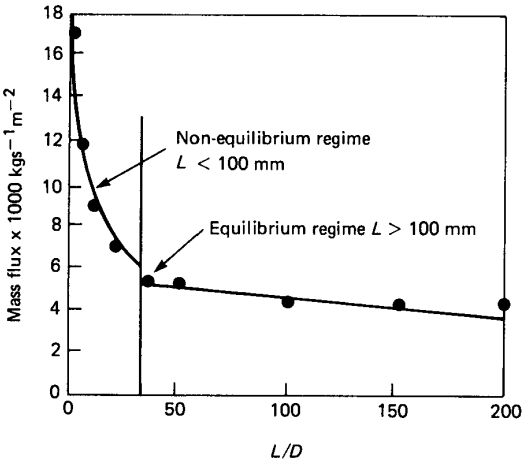

Figure 2 Saturated F-11 mass flux variation with L/D for $D = 3.2$ mm (Ref. 8), and comparison with calculated values (Equations (9) and (11)): •, experimental data, $P_0 = 4$ atm; —, calculated values

a parameter N in Equation (6)

$$G \approx \frac{h_{fg}}{v_{fg}} \left(\frac{1}{NTc}\right)^{1/2} \approx \frac{dP}{dT} \left(\frac{T}{Nc}\right)^{1/2} \tag{11}$$

where N is given by

$$N = \frac{h_{fg}^2}{2\,\Delta P\,\rho_f c_D^2 v_{fg}^2 Tc} + L/L_e \text{ for } 0 \leqslant L \leqslant L_e = 0.1 \text{ m} \tag{12}$$

where ΔP is the total available pressure drop and L (m) is the flow length. Equation (12) simply reflects that the degree of non-equilibrium is taken to vary directly with the fluid residence time, i.e. with duct length L.

For $L/D = 0$, the residence time is zero resulting essentially in no flashing, and Equations (11) and (12) reduce to the well known orifice equation for incompressible flow, i.e. $G = 0.6\sqrt{2\,\Delta P \rho_f}$.

Typical comparisons between predicted values from Equations (9) and (11) and experimental data covering both the non-equilibrium and equilibrium flow regimes are shown in *Figure 2*.

Model of the range of a volatile liquid jet

It is now well established that if a liquid is heated to above its boiling point at atmospheric pressure and released into the atmosphere, it disintegrates into fine droplets in the 10–100 μm size range[9]. Such small droplets will become airborne as a result of the momentum of the release and wind. This kind of dispersion is produced with relatively little superheat, and superheat seems to be the only requirement for a high degree of dispersion. Under ideal laboratory conditions, the data show that the amount of superheat that can be tolerated by a single phase, smooth orifice flow of liquid is given by the equation $(T_{sh} - T_{sat})/T_{sh} = 0.1$, where T_{sh} and T_{sat} are the jet shatter and saturation temperatures, respectively. In practice the actual superheat ratio approaches zero owing to aerodynamic-induced breakup, vapourization upstream of the discharge orifice, and the roughness of the orifice. Thus available experimental evidence leads to the conclusion that the atmospheric release of a liquid heated above its boiling temperature results in a two-phase plume of vapour and fine droplets.

Choked, liquid or two-phase jets are characterized by a rapid depressurization to or slightly below ambient pressure within approximately two break diameters from the outlet and very little mixing between jet and ambient over this distance. Downstream of the depressurization zone, the pressure within the jet may be taken to be constant and equal to the ambient pressure, and the flow within the jet is strongly influenced by an intensive exchange of mass with the atmosphere.

A sketch of the theoretical model of the jet is shown in *Figure 3*. The jet is divided into two regions: the depressurization zone, and the entrainment region in the far field. The evaporating jet is treated as a two-phase, axisymmetric free jet. A variable density single fluid model is employed to represent the actual liquid-vapour/air mixture. This assumption implies that the liquid and vapour phases move with the same velocity at any point within the jet, and that the specific heats and molecular weights of the air entrained by the jet are nearly equal to those of the evaporated liquid jet material. This is a limitation of the theory developed here. When this is not the case the air and the jet material have to be treated separately, but even then the present theory at least earmarks the important non-dimensional variables and provides some information on the details, such as the overall length of the two-phase region.

The sharp front depicted in *Figure 3* that separates the region of depressurization from the mixing region is somewhat unphysical. Observations of real jet behaviour indicate an intermediate zone where the jet radius is nearly constant and the pressure falls below the ambient value. Unfortunately, in the absence of quantitative information on the structure of this region, there is little alternative but to ignore it. We will first examine the depressurization region. This will provide the initial conditions for the entrainment region model that follows.

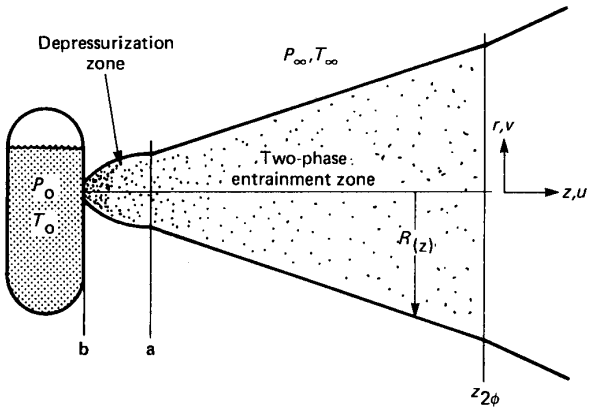

Figure 3 Sketch of the theoretical model

Depressurization region

Consider a high-pressure liquid or two-phase single-component jet discharged with velocity u_b through a circular break of flow area A_b. Friction, heat and momentum exchange with the ambient environment at pressure P_∞ are assumed to be negligible. Homogeneous equilibrium flow is assumed. Completion of the depressurization occurs when pressure equilibrium between the flow within the jet and the surrounding ambient is achieved. At this location the jet is fully expanded to its 'asymptotic' jet properties designated by the subscript 'a' (see *Figure 3*). The principle of conservation of momentum flux provides a simple relation between the asymptotic jet velocity u_a and the break plane quantities u_b, P_b, ρ_b and G_b, namely:

$$u_a = u_b + \frac{P_b - P_a}{\rho_b u_b} = u_b + \frac{P_b - P_a}{G_b} \tag{13}$$

This expression for the mean value of the maximum (asymptotic) jet velocity was first derived by Zerkowitz[10].

The asymptotic mass fraction of the vapour component within the jet can be estimated from the one-dimensional energy equation:

$$h_0 = h_f(P_\infty) + x_a h_{fg}(P_\infty) \tag{14}$$

where h_0 is the stagnation specific enthalpy (see *Figure 3*). Note that the kinetic energy of the jet at the end of the depressurization zone, $1/2\ \rho_a u_a^2$, is not included in Equation (14). This term is typically quite low for expanding two-phase jets. For an all liquid discharge, Equation (14) becomes:

$$x_a = \frac{c(T_0 - T_{bp})}{h_{fg}} \tag{15}$$

The area (or radius) of the jet at the start of the entrainment zone, A_a, is related to the area of the break A_b through the equation for the conservation of mass:

$$A_a = \frac{A_b u_b \rho_b}{u_a \rho_a} = \frac{A_b G_b}{u_a \rho_a} \tag{16}$$

where the asymptotic jet density, ρ_a is given by the definition:

$$\rho_a = \frac{1}{\dfrac{x_a}{\rho_g(P_\infty)} + \dfrac{1 - x_a}{\rho_f(P_\infty)}} \tag{17}$$

The above equations, together with the two-phase critical flow models for G_b discussed previously, provide the input data for the determination of the downstream jet behaviour, to which we now turn our attention.

Entrainment region

Before we begin to analyse the entrainment region, it is appropriate to introduce a related topic, the condensation of a submerged turbulent vapour jet. Reduced to its simplest form, the problem is to determine the penetration length achieved by the vapour jet before complete condensation upon the host, subcooled liquid of the same material. An attempt to provide a semi-empirical solution to the condensing jet problem has been made by Weimer *et al.*[11]. The starting point of their analysis is the conservation laws for mass, momentum and energy for the constant pressure entrainment region. Of course, in the case of a condensing vapour jet the entrained material is the surrounding subcooled liquid, whereas for the evaporating liquid jet of interest here, the warm ambient gaseous atmosphere is the material 'pulled' into the jet. The conservation equations written[11] pertain to a variable density, single fluid model. Recall that this assumption is embraced here. The authors proceeded by postulating 'top hat' density, velocity and enthalpy profiles to yield ordinary differential equations. Finally they adopted the entrainment law developed by Ricou and Spalding[12], based on measurements of entrainment with gas jets having a density different than the ambient gas.

It is known from the work of Ricou and Spalding[12] that the mass entrainment flux $\dot{m}_{ent}$ varies with the product of the local jet velocity u and the square root of the ratio of the density of the jet, ρ, to that of the surrounding gas, ρ_∞. The entrainment law is:

$$\dot{m}_{ent} - E_0 \rho_\infty u (\rho/\rho_\infty)^{1/2} \tag{18}$$

where E_0 is the so-called entrainment coefficient and for single-phase forced-convection jets $E_0 \approx 0.08$ (Ref. 12). The above expression is essentially a two-phase version of the expression proposed by Morton *et al.*[13] for turbulent jets driven by buoyancy. A similar expression has been employed to analyse liquid jets and boundary layers pumped by rising gas bubbles[14,15]. In work on forced turbulent jets, Morton[16] found that if top-hat profiles are used, $E_0 - 0.116$ results in the best agreement between theory and experiment. This value of E_0 will be emphasized in our numerical computations.

The consequence of the above described model of condensing vapour jets is a closed form solution for the variation of jet velocity u, enthalpy h, and radius R with axial distance z (Ref. 11). It can readily be shown, and perhaps is intuitively obvious, that the governing equations developed for the two-phase single-fluid condensing jet model are identical in form to the two-phase single-fluid evaporating jet model. Thus the solutions* for the evaporating jet u, h and R are the same as that obtained previously[11], and are:

$$\frac{u}{u_a} = \frac{h - h_\infty}{h_0 - h_\infty} = \frac{R_a}{R}\left(\frac{\rho_a}{\rho}\right)^{1/2} = \left(1 + 2E_0\left(\frac{\rho_\infty}{\rho_a}\right)^{1/2}\frac{z}{R_a}\right)^{-1} \tag{19}$$

In adopting these equations we have assumed that atmospheric turbulence and buoyancy may be neglected

* It should be noted that the experimental work of Weimer[11] on the penetration of submerged sonic vapour jets suggests an effective entrainment coefficient $E_0 \approx 0.014$. This value is considerably lower than $E_0 \approx 0.1$ inferred from experiments on single phase jets or two-phase bubble-liquid plumes. Presumably, the momentum dominated, depressurization region is relatively long within submerged condensing jets compared with that for conventional jets.

in comparison with the effects of turbulence and momentum generated by the discharge. Obviously, far downstream from the break, beyond the two-phase entrainment zone, environmental turbulence and buoyancy dominate the jet's motion. In the complete absence of a wind, the jet mixing with the atmosphere is entirely self-generated. For the purpose of obtaining a simple result for the length of the two-phase region, these assumptions appear to be reasonable.

It is important to recognize that Equation (19) cannot be used to predict the variation of u, h, R or ρ with axial distance z from the break. This is because the present single fluid model cannot distinguish between entrained air and evaporated liquid material within the jet. That is, even after invoking thermodynamic equilibrium, the fraction of gaseous material that is in equilibrium with the liquid as opposed to that fraction that is inert remains unknown. However, the model can be used to determine the length or range of the two-phase region.

The situation considered here involves a liquid-vapour mixture at its boiling point T_{bp} at the start of the entrainment region. The liquid is volatile, so that $T_{bp} < T_\infty$. Within the context of the model, the jet is uniformly mixed, and the two phases within the jet remain at T_{bp} until the liquid evaporation process is completed. The increase in the mean jet enthalpy through mixing with air is then reflected only by an increase in the mean vapour fraction within the jet. There are two reasons for questioning this assumption. First, the warm air entrained by the jet may conceivably raise the temperature of the vapour phase above T_{bp}. Second, since the droplets that comprise the liquid phase are continually decreasing in size by evaporation, the temperature of the liquid phase can fall well below its boiling temperature by evaporative cooling. (An approximate analysis that predicts the lower bound to the temperature of the liquid phase is given later.) The wide possible difference between the vapour and liquid temperatures would seem to justify a rational quantitative treatment of a two-phase jet. Unfortunately, calculation of the actual vapour and liquid temperature profiles entirely from first principles is rarely possible due to considerable numerical difficulties[17]. Accordingly, the temperatures of the liquid and gaseous phases are taken to be equal to the liquid boiling temperature. Once the enthalpy of the jet reaches the enthalpy of pure vapour, air and vapour being essentially the same species, the mean fraction of liquid is zero. Thus, the two-phase length of the jet, $z_{2\phi}$, is determined by setting $h = h_g(T_{bp})$ in Equation (19). This results in

$$\frac{z_{2\phi}}{R_a} = \frac{1}{2E_0}\left(\frac{\rho_a}{\rho_\infty}\right)^{1/2}\left(\frac{h_0 - h_\infty}{h_g(T_{bp}) - h_\infty} - 1\right) \tag{20}$$

The quantity h_∞ is the enthalpy of the gaseous species, vapour or air, evaluated at the atmospheric temperature T_∞. Thus $h_\infty = h_g(T_\infty)$. Moreover, if the fluid that discharges from the vessel is all liquid $h_0 = h_f(T_0) = h_f(T_\infty)$, since the vessel's contents are typically at atmospheric temperature. Combining these identifications with Equation (20) and assuming constant specific heats gives:

$$\frac{z_{2\phi}}{R_a} = \frac{1}{2E_0}\left(\frac{\rho}{\rho_\infty}\right)^{1/2}\frac{(1 - x_a)h_{fg}}{c_{p,g}(T_\infty - T_{bp})} \tag{21}$$

for the two-phase length of the jet.

Equation (19) then leads immediately to:

$$\frac{u_{2\phi}}{u_a} = \left(1 + 2E_0\left(\frac{\rho_\infty}{\rho_a}\right)^{1/2}\frac{z_{2\phi}}{R_a}\right)^{-1} \tag{22}$$

$$\frac{R_{2\phi}}{R_a} = \left(\frac{\rho_a}{\rho_\infty}\right)^{1/2}\left(1 + 2E_0\left(\frac{\rho_\infty}{\rho_a}\right)^{1/2}\frac{z_{2\phi}}{R_a}\right) \tag{23}$$

for the velocity and the jet radius, respectively, at the end of the two-phase entrainment region.

Temperature of the liquid phase

The temperature of the liquid falls between two physical bounds. The boiling point of the liquid, T_{bp}, represents the upper bound. The lower extreme is that corresponding to the maximum possible diffusion-controlled droplet evaporation rate, or evaporative cooling temperature T_{ec}. After an initial unsteady period, the droplets that comprise the liquid phase of the jet approach a quasi-steady state in which the temperature of the droplet is uniform and the rate of heat convected to the liquid, $\dot{q}$, by the relatively warm entrained air is just sufficient to vapourize the liquid at a rate $\dot{m}$, i.e.

$$\dot{q} = \dot{m}h_{fg} \tag{24}$$

The quantities $\dot{q}$ and $\dot{m}$ can be written in terms of transfer coefficients of heat (Nusselt number, Nu) and mass (Sherwood number, Sh), respectively, with the result:

$$k_g(T_\infty - T_{ec})\frac{\ln(1 + B)^{Le}}{(1 + B)^{Le} - 1} \times Nu = h_{fg}\rho_g D \ln(1 + B) \times Sh \tag{25}$$

The mass transfer number B is given by:

$$B = \frac{Y_{eq}(T_{ec}) - Y_\infty}{1 - Y_{eq}(T_{ec})} \tag{26}$$

where $Y_{eq}(T_{ec})$ is the mass fraction of the vapour at the surface of the liquid phase corresponding to equilibrium there and Y_∞ is the vapour mass fraction at the jet boundary. Note that the functional form of Equation (25) is such that it includes the effect of high evaporation rate on the transfer coefficients. The quantities k_g, ρ_g, D and Le are the thermal conductivity, density, binary diffusion coefficient and Lewis number ($Le = \rho_g D c_{P,g}/k_g$), respectively, of the vapour-air mixture within the jet. Often $Le = 1$ is an acceptable approximation for binary gas mixtures. It follows that $Nu \approx Sh$. The quantity Y can be replaced by the mole fraction (or vapour pressure P) since air and vapour are assumed to be equivalent from a molecular point of view. Also, since there is no vapour in the ambient atmosphere, $Y_\infty = 0$. As a result of these approximations, Equation (25) simplifies to:

$$\frac{c_{P,g}(T_\infty - T_{ec})}{h_{fg}} = \frac{P_{eq}(T_{ec})}{P_\infty - P_{eq}(T_{ec})} \tag{27}$$

Equation (27) determines the steady-state 'evaporative cooling value' of the droplet temperature, T_{ec}. It is the temperature that the jet asymptotically approaches as z goes to infinity. At the start of the entrainment region, the liquid and its vapour are in equilibrium at the boiling temperature of the liquid, and no air is present in the jet. Further downstream, air is entrained by the jet. The vapour pressure within the jet near the surfaces of the liquid phase (droplets) is reduced as a result of dilution by mixing with air. This in turn causes the liquid to vapourize and cool. The liquid continues to cool by evaporation until the heat flux provided by the entrained air is large enough to arrest the falling temperature and achieve a quasi-steady evaporation process. Evaporative cooling can result in rather cold jets with quasi-steady temperatures that are well below the boiling point of the liquid.

Comparison with ammonia spill tests

Goldwire[3] has reported the results of a large-scale pressurized ammonia release test performed on the Frenchman Flat area of the Department of Energy's Nevada Test Site. Liquid ammonia at $T_0 = 297\text{K}$ (24°C) and pressurized to $P_0 = 1.4 \times 10^6$ Pa (204 psia) was allowed to escape from a tanker truck through a 0.0945 m diameter orifice plate. The ammonia release was horizontal and resulted in a heavier-than-air cloud moving parallel to and in contact with the ground.

As discussed earlier, the velocity of ammonia through the orifice plate can be based on an all-liquid Bernoulli type flow.

$$u_b = 22.7 \text{ m s}^{-1}$$

The heat capacity of liquid ammonia $c_{P,f} = 4.46 \times 10^3$ J kg^{-1}K^{-1} and the latent heat of evaporation $h_{fg} = 1.37 \times 10^6$ J kg^{-1} and boiling temperature $T_{bp} = 240$ K (−33°C) at one atmosphere. Thus, from Equation (15), we predict a jet quality at the end of the depressurization zone of:

$$x_a = 0.19$$

The asymptotic jet density ρ_a is, from Equation (17):

$$\rho_a \approx \frac{\rho_g(P_\infty)}{x_a} = \frac{0.89}{0.19} = 4.68 \text{ kg m}^{-3}$$

and the asymptotic jet velocity u_a is, from Equation (13):

$$u_a = 22.7 + \frac{0.968 \times 10^6 - 0.101 \times 10^6}{(603)(22.7)} = 86.04 \text{ m s}^{-1}$$

Finally, from Equation (16), the radius of the jet at the equation of the depressurization zone is:

$$R_a = R_b \sqrt{\frac{u_b \rho_b}{u_a \rho_a}} = 0.275 \text{ m}$$

We are now in a position to estimate the length of the ammonia droplet cloud $z_{2\phi}$ from Equation (21). The temperature of the air atmosphere during the test was $T_\infty = 306$ K (33°C). Using the estimates $\rho_\infty = 1.1$ kg m^{-3} and $c_{P,g} = 10^3$ J kg^{-1}K^{-1}, which represent the properties of the air atmosphere, and entrainment coefficient $E_0 = 0.116$, we obtain:

$$z_{2\phi} = 0.275 \left(\frac{4.68}{1.1}\right)^{1/2} \frac{(1.37 \times 10^6)(1 - 0.19)}{10^3(306 - 240)}$$

or

$$z_{2\phi} = 39.1 \text{ m}$$

This estimate appears to be inconsistent with the observations, as the cloud was observed to persist beyond 400 m (Ref. 3). It is highly probable, however, that condensed atmospheric water vapour was responsible for the visible fog aerosol beyond ≈ 40 m.

From Equation (22), a jet velocity:

$$u_{2\phi} = 4.14 \text{ m s}^{-1}$$

is predicted at the end of the two-phase entrainment zone, which is just about the ambient wind speed measured during the test. The experimental observations indicated that the jet slowed to the wind speed at some location well beyond 100 m from the discharge orifice. The predicted jet radius at the end of the two-phase zone is, from Equation (23):

$$R_{2\phi} = 11.8 \text{ m}$$

The effective circular cross-sectional area of the jet then is 109 m^2. At 100 m from the release the heavier-than-air cloud was semi-elliptical in cross section, 70 m wide and less than 6 m high (≈ 260 m^2).

Three thermocouples were placed at ground level at 3, 6 and 9 m downstream of the discharge orifice[3]. Some fraction of the released mass was intercepted by the ground and, accordingly, the thermocouples were submerged in pools of deposited liquid ammonia drops. A simple model is illustrated in *Figure 4* for estimating the location at which interception occurred. By ignoring the short axial extent of the expansion zone and assuming that the plume spread is linear with distance, it follows that portions of the plume are estimated to strike the ground 2.5 m from the release plane. This result is encouraging as the thermocouples indicated pool temperatures of −52°C, −58°C, and −63°C at the 3, 6, and 9 m locations, respectively. Presumably the deposition of cold ammonia droplets is responsible for the measured pool temperatures. As discussed previously, the droplet temperature decreases with distance from the source, owing to evaporative cooling. It may be

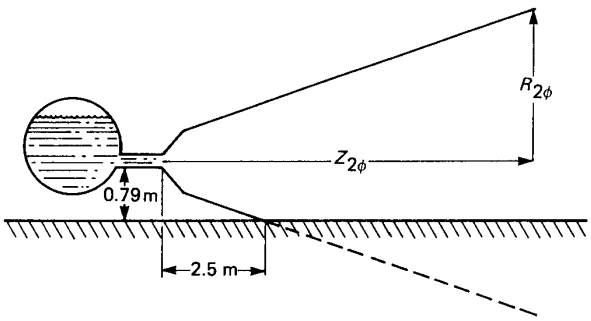

Figure 4 Prediction of point of interception of NH_3 aerosol cloud

Table 3 Examples of calculated lengths of ammonia and hydrofluoric acid aerosol (two-phase) jets and experimental observations

Fluid (reference)	Predicted length (m)	Experimental observations
NH_3 (Ref. 3)	38.4	Sharp increase in cloud temperature noted at less than 100 m downstream of the spill pipe (Ref. 20)
NH_3 (Ref. 18)	9.5	No ammonia pool on the ground at the point of interception of the plume approximately 10 m downstream of the spill pipe (Ref 18)
HF (Ref. 4) Spill Test No. 1	40.4	Sharp increase in cloud temperatures at about 40 m downstream of the spill pipe (Ref. 20)
HF (Ref. 4) Spill Test No. 3	23.6	Sharp increase in cloud temperature between 20 and 40 m from the spill pipe (Ref. 20)

calculated from Equation (27) that the liquid ammonia drops can cool to temperatures as low as:

$$T_{ec} = -75^{\circ}C$$

or 42°C below the liquid ammonia boiling point. A temperature level of 30°C below T_{bp} was measured in the pool located 9 m from the discharge orifice. This difference may be attributed to the presence of water vapour in the entrained air resulting in condensation and release of latent heat yielding higher T_{ec} values.

Ammonia plume measurements have also been recorded by Nyren and Winter[18]. Their spill facility resulted in a two-phase release of NH_3 from a 0.04 m diameter spill pipe located about 2 m above the ground and pointed horizontally. The measured two-phase discharge rate, density and pressure were 2.28 $kg\,s^{-1}$, 21.0 $kg\,m^{-3}$ and 0.226×10^6 Pa, respectively. Thus, from Equations (13), (15) and (17), we obtain the following asymptotic jet properties:

$$u_a = 155\ m\,s^{-1};\ x_a = 0.135;\ \rho_a = 6.59\ kg\,m^{-3}$$

and

$$R_a = 0.027\ m$$

From the measured atmospheric temperature of $T_\infty = 7.67^{\circ}C$ and Equation (21) we get:

$$z_{2\phi} = 9.5\ m \text{ and } R_{2\phi} = 2.27\ m$$

Thus the liquid ammonia component of the jet is predicted to be evaporated completely within 9.5 m of the break. Again assuming a straight-line plume expansion profile, the predicted point of plume interception by the ground is 9.7 m downstream. These calculated results are in excellent agreement with the observation that there were no signs of ammonia pools on the the ground at the point of interception of the plume approximately 10 m downstream of the spill pipe.

Comparison with hydrofluoric acid spill tests

Horizontal hydrofluoric acid spill tests were performed in 1986 at the U.S. Department of Energy Nevada Test Site[4]. Dispersion experiments 1 and 3 covered the range of experimental parameters and included spill pipe diameters of 1.65 and 0.953 in., respectively[19]. The ambient temperature was about 37°C for both spills with the liquid HF heated to 40°C. The spill rates for these tests are noted in *Table 1*. A humidification system was used during the third test in order to study the effect of the relative humidity (dew point of 7°C as compared with Experiment 1 with a dew point of −9°C)[19].

For spill Test No. 1 we obtain the following asymptotic jet properties from Equations (13), (15) and (16):

$$u_a \approx 27\ m\,s^{-1};\ x_a \approx 0.14;\ \rho_a \approx 20\ kg\,m^{-3}$$

and:

$$R_a \approx 0.13\ m$$

From the atmospheric temperature of $T_\infty = 37^{\circ}C$ and Equation (21) we obtain:

$$z_{2\phi} \approx 40.4\ m$$

Similarly for spill Test No. 3 we obtain:

$$u_a \approx 27.6\ m\,s^{-1};\ x_a \approx 0.14;\ \rho_a \approx 20\ kg\,m^{-3};$$
$$R_a \approx 0.076\ m$$

resulting in:

$$z_{2\phi} \approx 23.6\ m$$

The above calculated lengths of the hydrofluoric acid aerosol jets are summarized in *Table 3*, along with similar values for the previously noted ammonia spill tests. Based upon the various noted experimental observations listed in *Table 3*, the overall agreement with the data would appear to be quite satisfactory.

Finally, considerable cooling in connection with the entrainment process and vapourization is also noted for the hydrofluoric acid spill tests. Based on Equation (27) the liquid hydrofluoric acid drops can cool to about −25°C or 44°C below the liquid hydrofluoric acid boiling point. Experimental data suggest 39°C and 29°C below T_{bp} for spill Tests No. 1 and 3, respectively. The lower values, especially for spill Test No. 3 can be attributed to water vapour condensation and release of latent heat. This effect was ignored in deriving Equation (27). As noted earlier, the observed persistence of visible aerosol plumes well beyond the noted lengths in *Table 3*, is also due mainly to condensation of the atmospheric water content.

Conclusion

Much attention is being given to modelling the release and dispersion of toxic materials to the environment. While this topic is of great interest, it is important to

recognize that many emergency releases happen too fast to allow effective evacuation. Improvement of dispersion modelling would do little to further minimize consequences associated with Seveso and Bhopal type releases—if anything, it would reinforce the need to contain and/or mitigate such releases.

References

1 Fauske, H. K., 'Relief System Design for Runaway Chemical Reactions', Proc. Intl. Symp. On Preventing Major Chemical Accidents, Washington, D.C., USA, February 3–5, 1987
2 Fauske, H. K., 'Flashing Flows: Some Practical Guidelines for Emergency Releases', Plant/Operations Progress, 1985, **4** (3) 132–134
3 Goldwire, Jr., H. C., *Chem. Eng. Prog.* April 1986
4 Blewitt, D. N.. Yohn, J. F., Koopman, R. P. and Brown, T. C., Conduction of Anhydrous Hydrofluoric Acid Spill Experiments', Proc. Intl. Conf. on Vapor Cloud Modeling, Cambridge, MA, USA, November 2–4, 1987
5 Leung, J. C. and Grolmes, M. A., *AIChE Journal* 1987, **33** (3) 524–527
6 Fauske & Associates, Inc. Report, FAI/85-16 to AIChE DIERS, June 1983
7 Fauske, H. K., Loss Prevention Bulletin, IChemE, October 1987
8 Fletcher, B., 'Flashing Flow Through Orifices and Piles', AIChE 17th Loss Prevention Symp., Denver, CO, USA, August 28–31, 1983
9 Bushnell, D. M. and Gooderum, P. B. *J. Spacecraft and Rockets*, 1968, **5**, 231–232
10 Dryden, H. L., Murnaghan F. D. and Bateman H., in 'Hydrodynamics', Dover Publication, 1936, p. 540
11 Weimer, J. C., Faeth, G. M. and Olson, D. R., *AIChE Journal*, 1973, **19**, 552–558
12 Ricou, F. P. and Spalding, D. B. *J. Fluid Mech.*, **11**, 21–32
13 Morton, B. R., Taylor G. I and Turner J. S., *Proc. Roy. Soc.* 1956, **A23**, 1
14 Hussain, N. A. and Siegel R. *J. Fluids Eng.* 1976, **98**, 49–56
15 Cheung, F. B. and Epstein M. *Nucl. Eng and Design* 1987, **99**, 93–100
16 Morton, B. R. *J. Fluid Mech.* 1959, **5**, 151–163
17 Kansa, E. J. and Ermak, D. L., in 'Atmospheric Dispersion of Ammonia: An Ammonia Fog Model', (Ed. N. M. Faruklu) AIChE Symp. Series 1983, **225**, 79
18 Nyren, K. and Winger, S., 'Two-Phase Discharge of Liquified Gases Through Pipes. Field Experiments With Ammonia and Theoretical Model', Series from IChemE Symposium on Loss Prevention, Harrogate, UK, 1983
19 Koopman, R. P., personal communication, October 1987
20 Chan, S. T., Rodean, H. C. and Blewitt, D. N. 'FEM3 Modeling of Ammonia and Hydrofluoric Acid Dispersion', Proc. Intl. Conf. on Vapor Cloud Modeling', Cambridge, MA, USA, November 2–4, 1987